Proceedings of the 7th International Conference on the Application of Physical Modelling in Coastal and Port Engineering and Science (Coastlab18)
Santander, Spain, May 22-26, 2018

HYDRODYNAMICS UNDER LARGE-SCALE WAVES BREAKING OVER A BARRED BEACH

PIETRO SCANDURA[1], DOMINIC VAN DER A[2], JOEP VAN DER ZANDEN[3], CARMELO PETROTTA[4], CARLA FARACI[5], JAMES COOPER[6], SIMON CLARK[7], BJARKE ELTARD LARSEN[8], STEFAN CARSTENSEN[9], DAVID R. FUHRMAN[10], IVAN CACERES[11], STUART McLELLAND[12], GUILLAUME FROMANT[13], DAVID HURTHER[14], GERBEN RUESSINK[15], JOOST BRINKKEMPER[16] MING LI[17]

1 University of Catania, Italy, pscandu@unict.it 2 University of Aberdeen, UK, d.a.vandera@abdn.ac.uk
3 University of Twente, Netherlands, j.vanderzanden@utwente.nl 4 University of Messina, Italy, cpetrotta@unime.it
5 University of Messina, Italy, cfaraci@unime.it 6 University of Liverpool, UK, James.Cooper@liverpool.ac.uk
7 University of Liverpool, UK, S.D.A.Clark@liverpool.ac.uk 8 Technical University of Denmark, Denmark, bjelt@mek.dtu.dk
9 Technical University of Denmark, Denmark, scar@mek.dtu.dk 10 Technical University of Denmark, Denmark, drf@mek.dtu.dk
11 Polithecnic University of Catalonia, Spain, icaceres@upc.edu 12 University of Hull, UK, s.j.mclelland@hull.ac.uk
13 University of Grenoble Alpes; LEGI CNRS, France, guillaume.fromant@univ-grenoble-alpes.fr
14 University of Grenoble Alpes; LEGI CNRS, France, david.hurther@univ-grenoble-alpes.fr
15 Utrecht University, Netherlands, b.g.ruessink@uu.nl 16 Utrecht University, Netherlands, joost.brinkkemper@gmail.com
17 University of Liverpool, UK, m.li@liverpool.ac.uk

ABSTRACT

This paper shows preliminary results of experiments obtained in a large-scale wave flume under monochromatic waves plunging over a fixed bar. Velocity measurements were conducted using acoustic and optical instruments at 22 cross-shore locations ranging from the final part of the shoaling zone up to the inner surf zone. The measurements included the bottom boundary layer and the lower part of the water column and provided insights on the mean velocity distribution, turbulent velocity fluctuations and Reynolds stresses. The mean velocity is generally seaward directed. Magnitudes of the mean velocity are small in the shoaling region and increase above the bar crest, especially in the higher part of the water column, while magnitudes in the boundary layer are relatively small. Fluid from the inner surf zone is transported offshore by the undertow and pushed up near the shoreward face of the bar, thus largely feeding the onshore mass transport above trough level. As a result a large recirculation cell located just above the trough of the bar is generated where currents and turbulent velocity fluctuations are strong.

KEYWORDS: Breaking waves, surf zone, barred beach, turbulence, undertow.

1 INTRODUCTION

The coastal zone is one of the most dynamic areas of the earth, but it is also often highly populated and important for economic activities. It is particularly vulnerable to climate change effects such as sea level rise and increasing storm frequency which enhance coastal erosion. Hence, the availability of reliable morphodynamic models able to predict the impact of future climate change scenarios on the coast is crucial. The development of such models requires a full understanding of the hydrodynamic phenomena that occur in the coastal zone. In this regard, the surf zone is an area that is still subject to important deficiencies in terms of understanding for a number of reasons. In particular, wave breaking, which involves the sudden generation of vorticity and turbulence spanning over a wide range of spatial- and temporal scales, is still poorly understood. Furthermore, the strong unsteadiness and spatial variability of the flow field generated within the surf zone makes it generally difficult to collect experimental data with appropriate temporal and spatial resolutions. Despite these difficulties, several researchers have studied the hydrodynamic processes in the surf zone and the scientific results achieved until the 1980's have been summarized by Peregrine (1983) and Battjes (1988).

One of the first experiments involving detailed velocity measurements in the surf zone was carried out by Nadaoka *et al.* (1982) using a laser Doppler velocimeter (LDV). They observed no correlation between strong turbulence near the bed and the wave phase. This was explained using the assumption that turbulence generated by wave breaking was transported down to the bottom. Okayasu *et al.* (1986) obtained velocity measurements under plunging waves by using a hot film probe and an LDV. They deduced the existence of a large-scale vortex near the bed, just after plunging, and noted that the oscillating component of the velocity must contain an important rotational part.

Nadaoka *et al.* (1989) reported on characteristic vortex structures referred to as 'horizontal eddies' and 'obliquely descending eddies' which, according to the authors, have a major role in the generation of the Reynolds stress and in entraining and re-suspending sediments. Ting and Kirby (1994; 1995) also provided insights on the subject through the

analysis of velocity and turbulence measurements obtained by means of LDV. They reported that turbulent kinetic energy is transported landward under a plunging breaker and dissipates within one wave cycle. In contrast, under spilling breakers turbulent kinetic energy is transported seaward by the mean flow and the dissipation rate is much slower. In the bore region of a plunging breaker the velocity is slightly higher under the crest compared to the trough, but the turbulence is much higher under the crest, so on average turbulence is transported onshore. The temporal variation of turbulence under spilling breakers is relatively small, but the offshore-directed velocities are of higher magnitude and longer duration, so the net transport is offshore directed. Ting and Kirby (1996) provided further insights into the hydrodynamics of spilling breakers identifying that turbulent transport processes in this case are similar in the outer and inner surf zones and turbulent diffusion is the primary mechanism for transport with advection mainly being important near the surface.

From field measurements Ruessink (2010) showed that in the surf zone the Reynolds shear stress, which involves the correlation between the cross-shore and the vertical turbulent velocity fluctuations has the opposite sign to that of a boundary layer generated Reynolds stress. This result was explained by the presence of breaking induced vortices similar to those discussed by Nadaoka *et al.* (1989). Govender *et al.* (2002) highlighted that the region of highest turbulence production is located in the front part of the wave crest, close to the roller. Near the free surface turbulence has a clear phase dependence but this does not occur near the bed. Further contributions to the understanding of turbulence dynamics under breaking waves have been provided by numerous studies such as Cox and Kobayashi (2000), De Serio and Mossa (2006), Huang *et al.* (2009), and Sumer *et al.* (2013), which also highlighted the differences between spilling and plunging breakers in terms of turbulence dynamics.

All the studies described above, except the field measurements of Ruessink (2010), were based on experiments involving breaking waves over a plane sloping beach. The case of a barred beach is more interesting since it frequently appears in nature, thus it provides an improved understanding of the hydrodynamics over real beaches.

Smith and Kraus (1991) showed that the macroscopic features of waves breaking over plane and barred beaches are substantially different. Scott *et al.* (2005) carried out experiments in a large-scale wave flume involving waves breaking on an artificial barred beach which reproduced one of the profiles detected during the DUCK1994 field experiments. In these experiments breaking wave turbulence was maximum at the bar crest. Onshore from the crest, turbulence was mainly confined to the free-surface. Yoon and Cox (2010) performed velocity measurements in a large-scale wave flume over an evolving sandy beach which developed a bar. The authors observed that for an equilibrium beach state, mean turbulent kinetic energy and dissipation at the bar trough were smaller than those in the surf zone. Govender *et al.* (2011) measured the velocity field produced by plunging waves over a barred beach by means of a video-based digital correlation velocimeter. After plunging near the bar crest the waves transformed into a spilling breaker with turbulence confined in the upper part of the water column. Compared to spilling breakers on a plane beach the turbulence transfer towards the bed was significantly reduced.

Brinkkemper *et al.* (2016) studied the vertical structure of the turbulence in the surf and swash zones. In the surf zone they observed high turbulence levels during the phase at which the plunging jet hits the water surface. The process by which turbulence generated by wave breaking affects the boundary layer was studied by van der Zanden *et al.* (2016) who performed velocity measurements in the CIEM large-scale wave flume under plunging breaking waves propagating over a sandy, barred bed profile. In these experiments turbulence in the boundary layer showed peaks at two phases of the wave cycle: the first time when the wave plunges and the second time during the trough phase when turbulence is advected offshore by the wave and undertow velocities. Recently, van der A *et al.* (2017) discussed measurements carried out in the same wave flume and with the same experimental conditions considered in van der Zanden *et al.* (2016), except that the bed which was fixed by applying a layer of concrete. High values of the mean turbulent kinetic energy were observed on the onshore side of the bar where the jet penetrates into the water column. A strong upward advection of turbulent kinetic energy was also observed due to the undertow. Measurements during the same experiment were used in van der Zanden *et al.* (2018) to systematically explore the turbulent kinetic energy budget near the bed at 12 cross-shore locations. The analysis showed that production, dissipation, and advection were the primary terms driving the spatial and temporal variation in turbulent kinetic energy. Turbulence production rates near the bed are much higher in the breaking region than in the shoaling zone, due to the strongly non-uniform flow across the bar in combination with the presence of large-scale breaking-generated vortices.

Despite the recent large-scale research that has added new insights on the surf zone hydrodynamics, wave breaking remains a poorly understood phenomenon as highlighted above, particularly the effects of breaking on the near bed hydrodynamics. Few wave conditions and a limited portion of the surf zone have been analyzed to date, thus it is largely unknown how the geometrical and hydrodynamic parameters affects production and transport of turbulence. The experiments described herein were designed to expand the database generated in previous experiments (van der Zanden *et al.* 2016; van der A *et al.* 2017; van der Zanden *et al.* 2018). This goal has been achieved by generating new wave conditions, increasing the bed roughness, increasing the number of measurement locations and using new high precision optical instruments. This present paper discusses the preliminary results of these experiments, carried out in the large-scale CIEM wave flume, making use of the same bed profile used in van der A *et al.* (2017).

2 EXPERIMENTAL SET-UP AND PROCEDURES

The experiments were conducted in the CIEM large-scale wave flume at the Polytechnic University of Catalonia in Barcelona (Spain). The wave flume is 100 m long, 3 m wide and 5 m deep. The experiments were conducted at large

scale to generate a boundary layer flow with a Reynolds number that is similar to field conditions. As a result, scale effects on the bottom boundary layer flow, which are inherent to small-scale laboratory experiments, are minimized in the present study. The bed was constructed from concrete with a layer of gravel with D_{50}=0.009 m glued onto the surface to increase and homogenize the roughness. The bed profile was generated in a previous experiment (van der A *et al.*, 2017) and consisted of an offshore slope with a breaker bar and trough (Figure 2a). The origin of the reference system lies on the still water level, at the stroke centre of the wave paddle. The cross-shore *x*-axis is positive in the onshore direction. The spanwise *y*-axis has the origin at the right-hand wall when facing the beach and it is directed towards the left-hand wall. Finally, the *z*-axis is vertical and upward directed. The velocity components along the *x*, *y* and *z* directions are denoted as *u*, *v* and *w* respectively. In all the experiments the water depth in the deeper part of the wave flume was 2.65 m. The offshore slope is 1:12, it begins at *x*=34.2 m and ends near the bar crest at *x*=54.3 m. The height of the bar was 0.65 m from the trough to the crest. Onshore from the bar the profile slopes at 1:127 for 10 m and ends with a 1:7 sloping beach approximately 8 m long. All the results presented in this paper concern a monochromatic wave regime with period *T*=6 s and wave height *H*=0.55 m.

Two laser Doppler anemometers (LDAs), two acoustic Doppler velocimeters (ADVs), one acoustic Doppler velocity profiler (ADVP, described fully in Hurther *et al.*, 2011), two electromagnetic flow meters (EMCs) and a vectrino profiler (VP) were used for velocity measurements. The results here presented are based on measurements obtained using LDAs and ADVs. Data measured by means of ADVP have been used to replace some missing data from LDAs and ADVs. The LDAs measured the *u* and the *w* velocity components at a sampling frequency of 300 Hz on average. These rates varied dependent on the concentration of seeding particles and on the fluid velocity. The ADVs and the ADVP measured the three velocity components at a sampling frequency of 100 Hz and 25 Hz respectively. These instruments were deployed from a frame attached to a carriage placed on tracks at the top of the wave flume (see Figure 1). By moving the carriage along the horizontal direction and the frame along the vertical it was possible to obtain measurements at any positions along the profile.

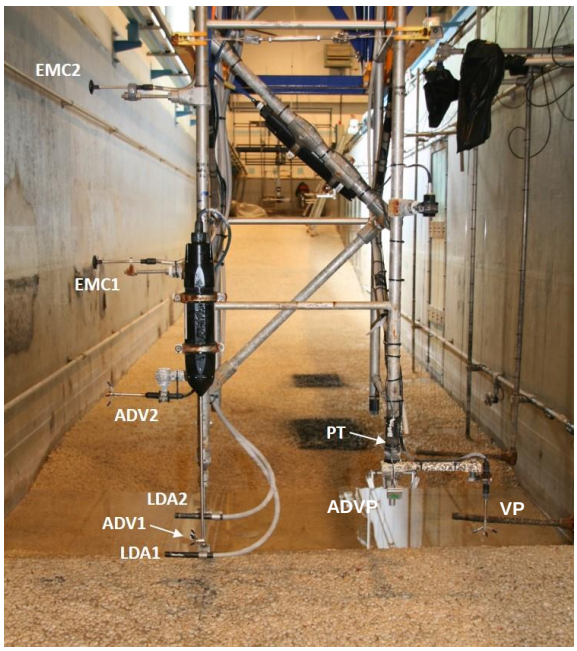

Figure 1. Photo of the mobile frame positioned above the bar crest including the measurement instruments.

The flow velocity was measured at 22 cross-shore locations in the range *x*=49-64 m. For each cross-shore position, the frame was positioned at three different elevations, yielding velocity measurements by the LDAs and ADVs at 12 elevations, in addition to the ADVP measurements which covered a 0.15 m profile above the bed with 1.5 mm vertical bin size resolution. Additional detailed measurements of the WBL flow were obtained at *x*=50.78 m. These velocities were measured with the LDA at 16 vertical positions, starting from 0.005 m up to 0.125 m from the top of the bed roughness and logarithmically spaced to capture the velocity distribution within the boundary layer. At each cross-shore position of the frame, waves were generated for approximately 45 minutes. Measurements were obtained for a duration of 12 min at each elevation, corresponding to approximately 120 waves.

The water surface elevation was measured at 12 cross-shore locations by means of resistive wave gauges (RWG) and at 52 locations by means of acoustic wave gauges (AWG). In addition, 12 pressure transducers (PT) were used to determine the water surface elevation with linear wave theory. All these instruments measured the water surface elevation at a frequency of 40 Hz.

Within the wave flume statistically steady conditions were generally established approximately 300 s after the wave paddle started. This time was evaluated by analyzing the temporal developments of the water surface elevations and the velocity at different cross-shore and vertical positions. After discarding the first 300 s the remaining time series were used to compute the velocity and water surface statistics. In all the cases the statistics were computed on the basis of no less

than 100 waves. The ensemble average was determined as follows:

$$\langle u \rangle = \frac{1}{N} \sum_{n=0}^{N-1} u(t + nT), \tag{1}$$

where T is the wave period, and N the number of waves included in the computation of the ensemble average. The wave period was evaluated from the water surface elevations measured with the resistive wave gauge located at x=50.85 m. The wave period T was computed as the arithmetic average of the periods of about 100 waves obtained by applying the zero up-crossing technique to the water surface elevation time series. In all the runs the standard deviation of T was approximately 6×10^{-3} s, thus confirming that the periods exhibits only a very small wave-to-wave variation, which allows using a constant value for T in the averaging procedure. Expressions analogous to (1) were used to compute the ensemble average of the other velocity components and for the free surface elevation.

The non-equidistant sampled LDA measurements were phase-averaged, accounting for particle residence time to prevent velocity bias. The instantaneous velocity u can be written as follows:

$$u = \bar{u} + \tilde{u} + u', \tag{2}$$

where the bar denotes a time average, the tilde denotes the periodic fluctuating term of the ensemble average and the prime denotes the turbulent component ($\langle u \rangle = \bar{u} + \tilde{u}$).

3 RESULTS

3.1 Water surface elevation

Figure 2 shows the bed profile, wave height, the mean water surface elevation (set-up/set-down) and the root-mean-square (rms) of the water surface elevations along the wave flume. The wave overturning which leads to breaking begins at x=53.50 m approximately (see 'breaking point' in figure 2a). At x=55.50 m the wave overturning is completed (see 'plunging point' in figure 2a) and the plunging jet hits the free surface causing a localized transfer of momentum to the water column. As a consequence a new wave is generated which very rapidly becomes a stable roller that propagates towards the beach.

The wave height is close to 0.55 m in the horizontal part of the wave flume but figure 2b shows that it oscillates along x. A rough estimate of amplitude and wavelength of these oscillations shows that they are approximately 0.12 m and 15 m respectively. These oscillations are likely due to wave reflection from the beach, which generates partial standing waves whose envelop of wave heights has a wavelength equal to half the wavelength of the incident progressive wave. This explanation is consistent with the estimated wavelength of the progressive waves, which is equal to 30 m approximately. However, the reflection does not have a significant effect on the processes that occur in the surf zone which are characterized by intense energy dissipation.

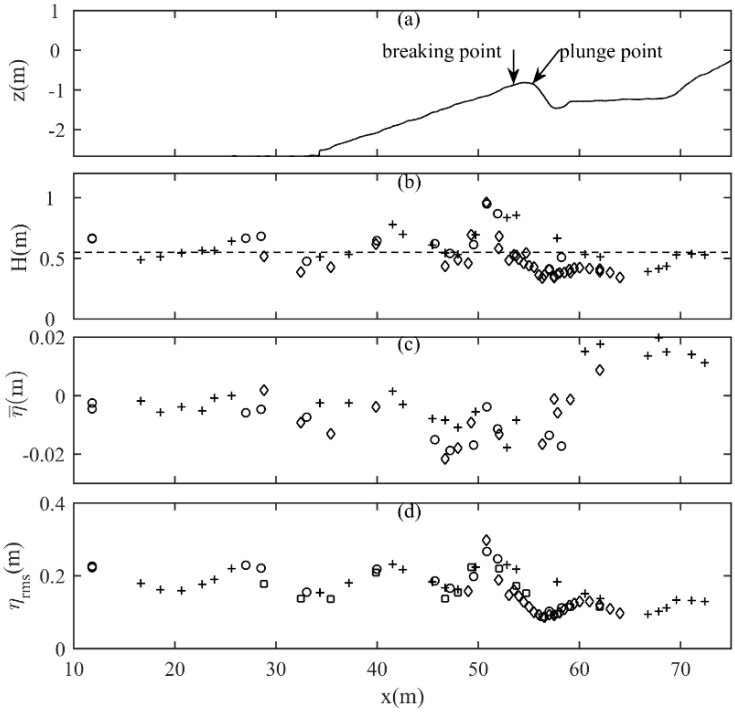

Figure 2. Wave characteristics along the wave flume measured by resistive and acoustic wave gauges and pressure transducers. (a) Bed profile of the wave-flume; (b) wave height; (c) mean water level; (d) rms of the free surface elevation. ○ Resistive wave gauges; + acoustic wave gauges; ◊ pressure transducers.

The mean water level (Figure 2c) is approximately equal to zero up to x=40 m. Then a set-down begins which lasts up to x=55.50 m approximately. Although within the range x=40-55.50 m the data are rather scattered, it can be appreciated that the set-down is about -0.01 m on average. The mean water level $\bar{\eta}$ starts to increase near x=55.5 m, which is the location where the plunging jet hits the water surface. This increase in mean water level is a result of the decrease of the onshore momentum flux due to the wave energy dissipation, which must be balanced by a positive cross-shore gradient in $\bar{\eta}$. The rms of the free surface elevation (Figure 2d) is about 0.2 m in the horizontal part and exhibits oscillations analogous to those observed for the wave height.

3.2 Time-averaged outer flow

The velocities used for the spatial representation of the time-averaged cross-shore velocity $\bar{u}$ and vertical velocity $\bar{w}$ within the measurement region are those measured by LDA1, LDA2 and ADV2 which showed reasonable agreement among themselves. The data from ADV1 were discarded because, from the most offshore measurement location up to the bar trough, they showed a slight yet constant disagreement with those provided by the other instruments. This discrepancy can be attributed to the fact that the x position of ADV1 was about 0.17 m offshore with respect to that of the other instruments. Measurements carried out with ADVs are often affected by spurious data which appears in the form of spikes. When few, isolated spikes are present, the time series can be corrected. On the other hand when the spikes appear continuously during certain range of time the entire measurement must be rejected. The last condition occurred in some cases in the present experiments, due to significant air bubble presence and probe emergence. These spurious measurements as well as intervals of ADV probe emergence from the water could be well identified on the basis of a signal to noise ratio below 7 or a correlation value below 50%. Spurious data records due to isolated spikes were removed using a despiking routine based on phase-space and replaced through interpolation using cubic polynomial. Spurious velocity measurements above wave trough level were detected on the basis of signal to noise ratio and correlation and set to 0. Thus, mean velocities above to the trough level were computed over the full wave period.

In the two-dimensional plots presented in the figures below, nine measurements points distributed over the depth were used at each of the 22 cross-shore positions. These points were obtained by measuring the velocity at three different positions by means of LDA1, LDA2 and ADV2, with three different elevations of the frame at each cross-shore location. From the 198 measurement points, 10 data records were discarded because of instrument malfunctioning or poor data quality. To enable a constant number of points to be plotted along each vertical, these missing recordings were replaced by ADVP data or by means of interpolation from adjacent data. Replacing data by interpolation did not alter the main trend of the velocity distribution, since it was used only where the velocity was not subject to rapid changes, moreover the missing data records were few in comparison to the total number of recordings.

Figures 3 and 4 show the spatial distribution of the mean velocity in the x- and z-direction, respectively. At the most offshore shoaling zone locations, the mean velocity is small and almost constant with depth. At x=49 m for example, the velocity shows only small variations along z and takes values of -0.05 ms^{-1} approximately. This velocity is seaward directed in order to balance the landward mass transport near the water surface induced by the progressive wave. This onshore flux contribution is present in Figure 3 only at a few locations as measurements were mainly obtained in the lower part of the water column. The negative velocities increase further shorewards reaching values of -0.20 ms^{-1} around the bar crest at x=53.5 m, where the overturning process begins. The mean vertical velocity (shown in Figure 4) is rather small at these locations. From this point up to x=57.5 m the mean horizontal velocity slightly decreases in magnitude. At x=55.5 m the plunging jet hits the free surface and subsequently penetrates obliquely into the mass of water, transferring a large amount of momentum. Figure 4 shows that this momentum transfer gives rise to large negative mean velocities which reach the bed at x=58-60 m. The largest mean velocities in Figure 3 occur where the mean vertical velocity vanishes (Figure 4). This shows that in this region the offshore current grows in magnitude as long as there is a downward flux that feeds it. The upward flux close to the shoreward face of the bar balances this downward flux plus the undertow coming from the inner surf zone. Thus, it contributes to the establishment of a large scale circulation which allows landward mass transport to take place without violating mass conservation. Part of the fluid however remains trapped in a recirculation cell just above the bar trough. The maximum of both the mean cross-shore and vertical velocities are attained within this cell and are approximately 0.40 and 0.15 ms^{-1} respectively. In the inner surf zone (x>60 m) the offshore velocity is mostly constant and approximately 0.2 ms^{-1} even close to the bed, indicating that here the undertow has a strong impact on the boundary layer. In contrast, in the inner surf zone the mean vertical velocity is small (Figure 4), with magnitudes comparable to those in the shoaling region.

Figure 3 shows that over the onshore face of the bar (x=55.5 to 57.0 m) a small near-bed area is present where the mean velocity is positive while the velocity is negative at adjacent locations. The dynamic mechanism responsible for this positive mean velocity is not clear yet. From a kinematical point of view this positive velocity is due to the negative vertical velocity occurring offshore which extends up to the onshore face of the bar where, due to the inclination of the bottom, a positive u velocity component is generated. Continuity is satisfied since the upward current that occurs at x=57 m which brings the water towards the surface.

In Figure 5 the time-averaged rms of the cross-shore velocity fluctuations $\overline{u'_{rms}} = \overline{\langle u'^2 \rangle^{1/2}}$ is shown. In the shoaling region (x=49 m) $\overline{u'_{rms}}$ is ≈0.02 ms^{-1} and it is rather constant over depth, except close to the bed where the contribution from bed generated turbulence is important. On the bar, turbulence intensity increases up to 0.055 ms^{-1} on average. Here $\overline{u'_{rms}}$ attains the minimum in the middle of the water column at z=-0.6 m approximately. This is due to the coexistence of two main sources of turbulence: the boundary layer and the free surface. The highest measured values of $\overline{u'_{rms}}$ is ≈0.25 ms^{-1} and occurs at the highest measurement point at x=58.50 m, because of the direct impact of the plunging jet. The rms of u' is also large near the bed at x=57.5 m where it takes values of ≈0.15 ms^{-1}, but here turbulent fluctuations are mainly generated by boundary layer processes rather than the direct effect of wave breaking.

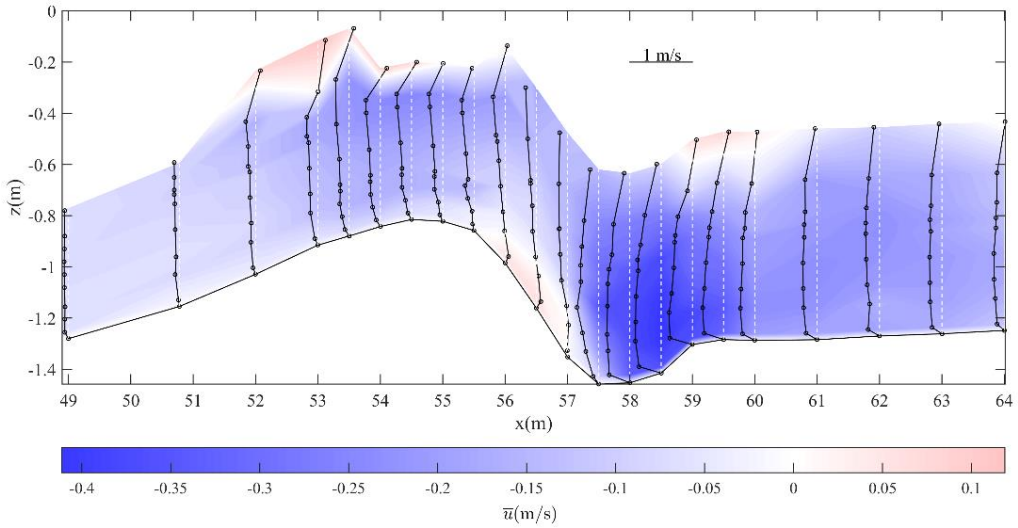

Figure 3. Time-averaged cross-shore velocity $\overline{u}$.

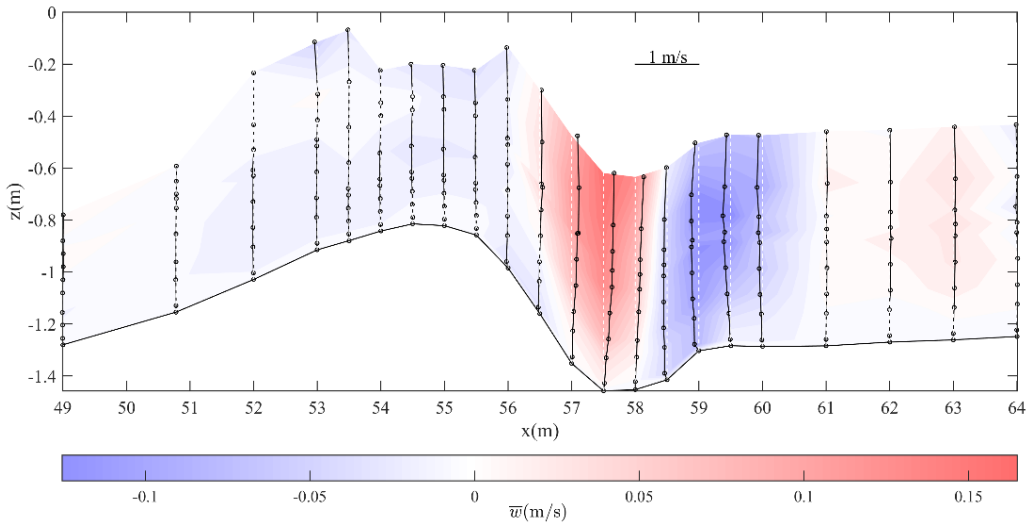

Figure 4. Time-averaged vertical velocity $\overline{w}$.

The time-averaged rms of the vertical velocity fluctuations $\overline{w'_{rms}} = \overline{\langle w'^2 \rangle^{1/2}}$, shown in Figure 6, is generally only slightly smaller than $\overline{u'_{rms}}$. For example, in the inner surf zone the maximum measured values of $\overline{u'_{rms}}$ and $\overline{w'_{rms}}$ are 0.15 and 0.12 ms^{-1} approximately. This result implies a certain degree of turbulence isotropy which certainly does not occur in the boundary layer. Similar to $\overline{u'_{rms}}$, $\overline{w'_{rms}}$ is very large above the trough of the bar with values of 0.22 ms^{-1}.

Another similar characteristic is the trend of the vertical profile on the bar crest which show a minimum close to z=-0.6 m. The main difference between $\overline{u'_{rms}}$ and $\overline{w'_{rms}}$ occurs near the bed. Indeed, the high values of $\overline{u'_{rms}}$ detected near the bed at x=57-58 m in Figure 5 are not observed for $\overline{w'_{rms}}$ in Figure 6 because of the near bed turbulence anisotropy.

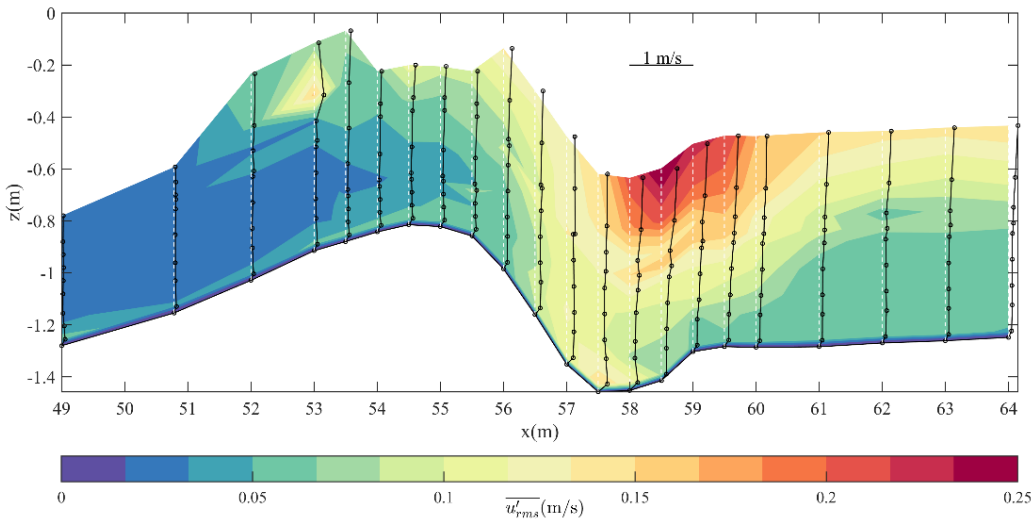

Figure 5. Time-averaged root mean square cross-shore turbulent velocity.

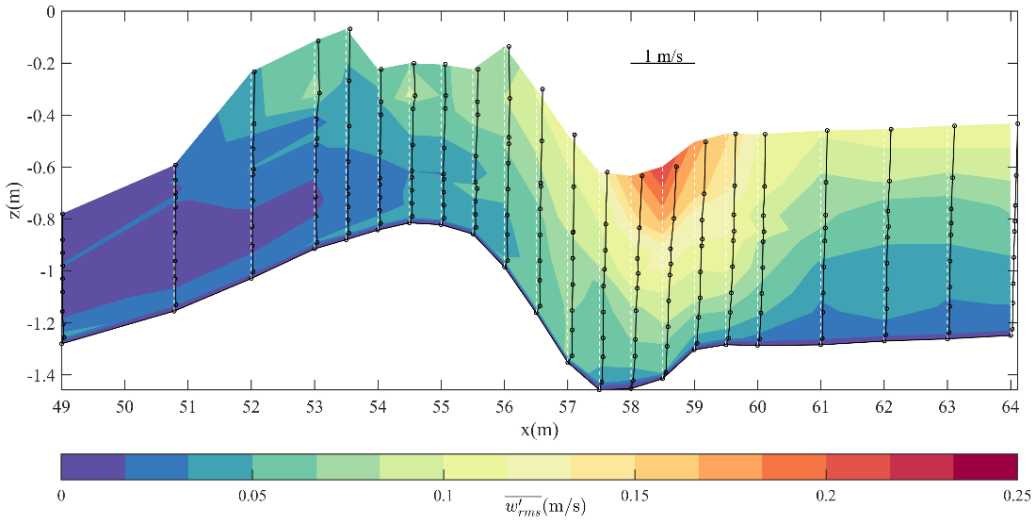

Figure 6. Time-averaged root mean square vertical turbulent velocity.

3.3 Boundary layer flow

The boundary layer flow was measured by means of LDA and ADVP, however only at x=50.78 m detailed measurements within the boundary layer carried out by means of LDA are available. This section is devoted to the analysis of the boundary layer measurements by LDA at x=50.78 m.

Location x=50.78 m is in the shoaling region, 4 m offshore away from the bar crest, thus at this location only an indirect effect of the breaking processes that occur further onshore may be detected. Figure 7a shows the time development of the free stream velocity measured at z'=0.125 m (z' is the distance from the top of the bed roughness). It can be observed that the free stream velocity has a large velocity skewness and acceleration asymmetry. The skewness *Sk* and the asymmetry *Asy* measure the departure of the free stream velocity from a sinusoidal function and are given as follows:

$$Sk = \frac{\overline{\tilde{u}^3}}{\overline{\tilde{u}^2}^{3/2}}, \qquad Asy = \frac{\overline{\dot{\tilde{u}}^3}}{\overline{\dot{\tilde{u}}^2}^{3/2}}, \tag{2}$$

where a dot denotes a time derivative. Skewness and asymmetry of the free stream velocity shown in figure 6a are equal to 0.93 and 1.45 respectively, due to the strong prevalence of positive velocities and accelerations compared to the negative ones. The Reynolds number R_δ of the boundary layer based on the maximum of the free stream velocity and on the thickness of the Stokes layer $\delta = \sqrt{\nu T/\pi}$ (ν is the kinematic viscosity) is equal to 1000 approximately. It decreases to 800 approximately if the Reynolds number is evaluated by means of the arithmetic average of the positive and negative velocity peaks. Considering that the roughness is made up by gravel with D_{50}=9×10^{-3} m, in all the cases the flow falls in the rough turbulent regime according to the classification of Jonsson (1980).

Figure 7 shows the free-stream velocity (plot a) and the vertical distributions of the time-averaged horizontal velocity at 7 stages of the wave cycle (plot b). The variability in the vertical profiles appears to be due to offsets in synchronization between the different acquisitions. Figure 7 shows that at t=0 the velocity rapidly increases and attains the maximum at

t=0.5 s. At this phase there is a well-defined overshoot in the velocity profile at z'= 0.02 m, probably enhanced by the convergence effect of the bed geometry. The Reynolds stress (Figure 8), which was positive everywhere at t=0 s, becomes negative near the bed at t=0.5 s and remains positive far from the bed. The positive Reynolds stress is due to the negative velocity gradient that occurs above the point of the velocity maximum while the negative part is due to the positive velocity gradient near the bed (z' < 0.02 m). After t = 0.5 s the velocity decreases but at t=1 s the Reynolds stress is larger than at t=0.5 s. At t=1.9 s the velocity is small and the Reynolds stress is reduced substantially near the bed. An increase of the velocity in the negative direction (t=2.5 s) causes an increase of the Reynolds stress which finally becomes positive at t=4.5 s when the maximum negative velocity is attained. Because of skewness and asymmetry, and because of the undertow, the mean velocity and the Reynolds stress do not vanish in the boundary layer. The mean velocity is negative at z'=0.12 m where it reaches its outer flow value of -0.05 ms^{-1} approximately. The mean Reynolds stress has a more intricate trend: below z'=0.007 m it is positive, then it becomes negative up to 0.025 m, at higher elevations it becomes positive again and finally tends asymptotically to zero far from the bed.

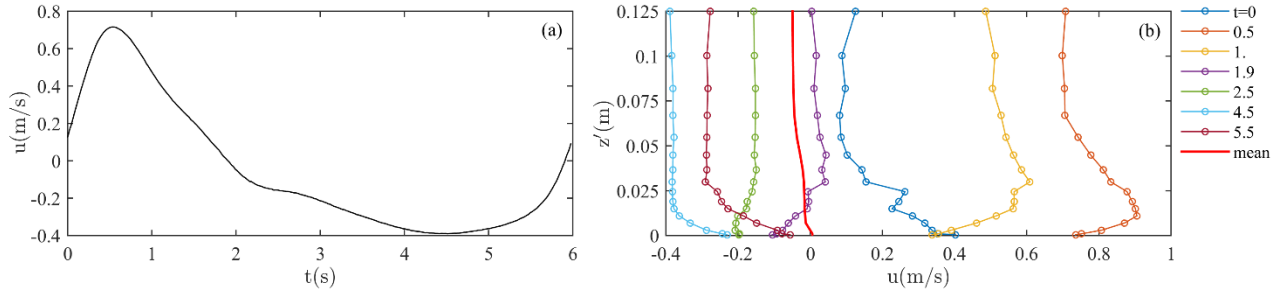

Figure 7. (a) Free stream velocity; (b) velocity profiles. x=50.78 m.

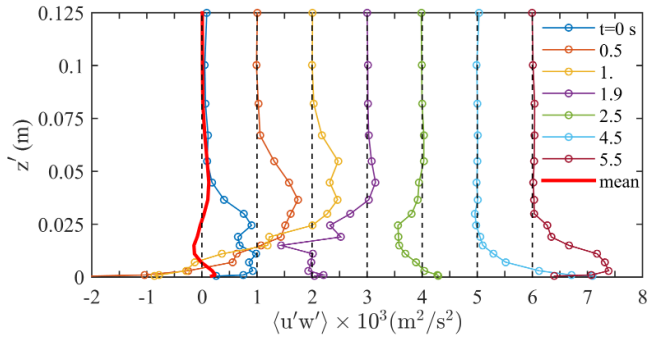

Figure 8. Reynolds stress at x=50.78 m. For clarity, the data of each phase are shifted forward by 10^{-3} m^2/s^2 with respect to those of the previous phase.

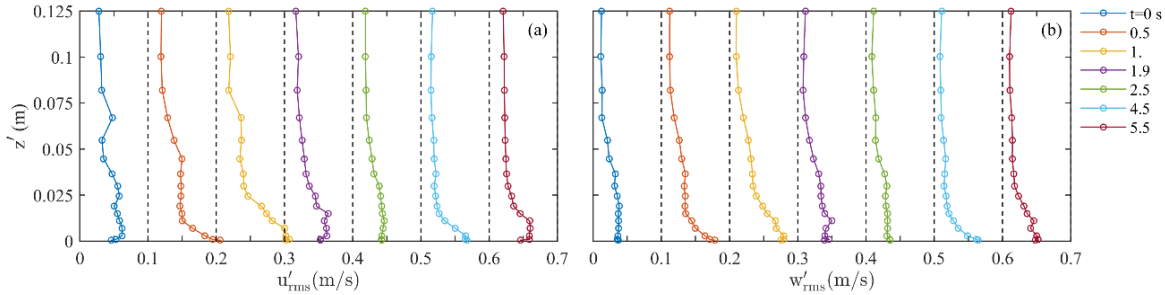

Figure 9. Turbulent intensities at x=50.78 m. (a) Cross-shore turbulent intensity; (b) Vertical turbulent intensity. The data of each phase are shifted forward by 0.1 ms^{-1} compared to those of the previous phase.

Figure 9 shows the rms of the cross-shore and vertical turbulent velocity fluctuations in the boundary layer. First of all it can be observed that in the boundary layer the cross-shore turbulent intensity is larger than the vertical turbulent intensity at all the phases. The turbulent intensities increase during the accelerating phase and become large at the peak of the free stream velocity (t=0.5 s). However, as already observed for the Reynolds stress, the turbulent intensities continue to increase during the decelerating phase and at t=1 s they attain values larger than those at the peak of the free stream velocity. Turbulent intensities during the onshore flow half-cycle are higher than those of the offshore flow half-cycle because of the flow skewness and asymmetry. The increase in turbulent intensity during the decelerating phase is analysed in Figure 10 which shows the temporal development of u'_{rms} at three different elevations, with the free stream velocity given as reference.

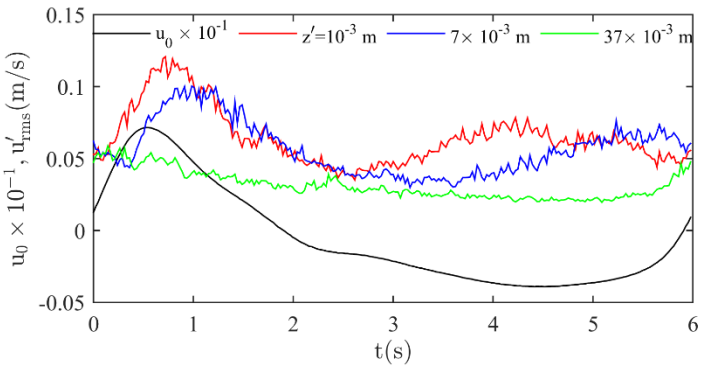

Figure 10. Time variation of u'_{rms} at three different elevations. The free stream velocity u_0 is shown as reference. x=50.78 m.

It can be seen that very close to the bed the first peak of u'_{rms} (red line) has a small delay with respect to the peak of u_0. It can be observed that because of this delay u'_{rms} at t=0.5 s is slightly smaller than at t=1 s. The difference between the two phases increases at higher elevation. Indeed at z'=7×10^{-3} m (blue line) the delay of the first peak increases and u'_{rms} at t=0.5 s further decreases significantly. Such a forward shift of the phase of u'_{rms} with z' is mainly due to turbulent diffusion and it has been observed also in numerical simulations (Scandura *et al.* 2016). At higher distance from the bed (z'=37×10^{-3} m) only one main peak is detected.

4 CONCLUSIONS

The flow velocity was measured with high spatial and temporal resolution under monochromatic waves plunging on a fixed barred beach in a large-scale wave flume. In the shoaling region the undertow velocity is small, while its magnitude increases on the bar crest where a velocity of -0.2 ms^{-1} is detected approximately 0.32 m below the still water level. On the bar crest the mean vertical velocity is small and does not exceed values of 10^{-2} ms^{-1}. Shoreward from the bar crest the mean horizontal offshore directed velocity slightly decreases in magnitude up to the trough of the bar where it suddenly increases in the lower part of the water column. At the same location, the mean vertical velocity component increases to allow the strong offshore fluid flux to be directed upward. This fluid flowing offshore comes mainly from the inner surf zone and when it is pushed up, near the shoreward face of the bar, it feeds the onshore mass transport that in turn feeds the undertow current. Part of the fluid however remains trapped in a recirculation cell located above the trough of the bar. Within this flow recirculation zone the mean velocities attain the largest values. In magnitude the maximum mean velocities are 0.4 ms^{-1} for the horizontal component and 0.15 ms^{-1} for the vertical. Where the plunged wave propagates in the form of a bore, the mean velocity is mostly constant along the cross-shore x direction and takes values of approximately 0.2 ms^{-1} until near to the bed, thus the boundary layer is strongly affected by the undertow.

The time-averaged cross-shore and vertical turbulent intensities are large within the recirculation cell above the bar trough, where they take maximum values of 0.25 and 0.22 ms^{-1} respectively. Generally, the two turbulent intensities differ only slightly; in the inner surf zone, for example, maximum measured values of $\overline{u'_{rms}}$ and $\overline{w'_{rms}}$ are approximately 0.15 and 0.12 ms^{-1} respectively.

Specific results concerning the boundary layer have been reported for a location corresponding to the shoaling region where detailed LDA measurements are available. The free stream velocity has a large velocity skewness and acceleration asymmetry. These characteristics combined with the flow convergence effect due to the bed slope result in a much more prominent overshoot in the onshore half-cycle velocity profiles compared to that in the offshore half-cycle. The Reynolds stress shows trends that are expected based on the velocity profiles: it is negative when the velocity gradient is positive and vice-versa, and it is very small outside the wave boundary layer. Near the bed, the Reynolds stress and the rms of the velocity fluctuations increase during the first part of the decelerating phase. The turbulence intensities show two peaks during the wave cycle, characterized by a depth-dependent time lag with respect to the free-stream velocity due to turbulent diffusion. These features of the boundary layer dynamics will be the subject of future work based on data acquired by the ADVP.

ACKNOWLEDGEMENT

This work is part of the transnational access project HYBRID supported by the European Community's Horizon 2020 Program through the grant to the budget of the integrated infrastructure initiative HYDRALAB+, Contract no. 654110. We are grateful to CIEMLAB staff Oscar Galego, Andrea Marzeddu, and Joaquim Sospedra for their technical support.

REFERENCES

Battjes, J. A., 1988. Surf-zone dynamics, *Annual Review of Fluid Mechanics*, 20, 257–293.

Brinkkemper, J. A., Lanckriet, T., Grasso, F., Puleo, J. A., Ruessink B. G., 2016. Observations of turbulence within the surf and swash zone of a field-scale sandy laboratory beach, *Coastal Engineering*, 113, 62–72.

De Serio, F., Mossa, M., 2006. Experimental study on the hydrodynamics of regular breaking waves, *Coastal Engineering*, 53(1), 99–

113.

Govender, K., Mocke, G. P., and Alport, M. J., 2002. Video-imaged surf zone wave and roller structures and flow fields, *Journal of Geophysical Research: Oceans*, 107(C7), 9-1–9-12

Govender, K., Michallet, H., Alport M. J., 2011. DCIV measurements of flow fields and turbulence in waves breaking over a bar, *European Journal of Mechanics B-Fluids*, 30(6), 616–623.

Huang, Z. C., Hsiao, S. C., Hwung, H. H., Chang K. A., 2009. Turbulence and energy dissipations of surf-zone spilling breakers, *Coastal Engineering*, 56(7), 733–746.

Hurther, D., Thorne, P. D., Bricault, M., Lemmin, U., & Barnoud, J. M., 2011. A multi-frequency Acoustic Concentration and Velocity Profiler (ACVP) for boundary layer measurements of fine-scale flow and sediment transport processes. *Coastal Engineering*, 58(7), 594-605. doi: 10.1016/j.coastaleng.2011.01.006

Jonsson, I. G., 1980. A new approach to oscillatory rough turbulent boundary layers. *Ocean Engineering*, 7(1), 109-152. doi:10.1016/0029-8018(80)90034-7

Nadaoka, K., Hino, M., Koyano, Y., 1989. Structure of the turbulent-flow field under breaking waves in the surf zone, *Journal of Fluid Mechanics*, 204, 359–387.

Peregrine, H., 1983. Breaking waves on beaches, *Annual Review of Fluid Mechanics*, 15, 149–178.

Ruessink, B. G., 2010. Observations of turbulence within a natural surf zone, *Journal Physical Oceanography*, 40(12), 2696–2712.

Scandura, P., Faraci, C., Foti, E., 2016. Numerical simulations of acceleration-skewed oscillatory flows, *Journal of Fluid Mechanics*, 808, 576-613.

Scott, C. P., Cox, D. T., Maddux, T. B., Long J. W., 2005. Large-scale laboratory observations of turbulence on a fixed barred beach, *Measurement Science and Technology*, 16(10), 1903–1912.

Shin, S., Cox, D., 2006. Laboratory observations of inner surf and swash-zone hydrodynamics on a steep slope, *Continental Shelf Research*, 26(5), 561–573.

Smith, E., Kraus N., 1991. Laboratory study of wave-breaking over fixed bars and artificial reefs, *Journal Waterway, Port, Coastal Ocean Engineering*, 117(4), 307–325.

Sumer, B. M., Guner, H. A. A., Hansen, N. M., Fuhrman, D. R., Fredsøe J. 2013. Laboratory observations of flow and sediment transport induced by plunging regular waves, *Journal of Geophysical Research*, 118, 6161–6182, doi:10.1002/2013JC009324.

Ting, F. C. K., Kirby, J. T., 1994. Observation of undertow and turbulence in a laboratory surf zone, *Coastal Engineering*, 24, 51–80.

Ting, F. C. K., Kirby, J. T., 1995. Dynamics of surf-zone turbulence in a strong plunging breaker, *Coastal Engineering*, 24, 177–204.

Ting, F. C. K., Kirby, J. T., 1996. Dynamics of surf-zone turbulence in a spilling breaker, *Coastal Engineering*, 27, 131–160.

Ting, F. C. K., Nelson J. R., 2011. Laboratory measurements of large-scale near-bed turbulent flow structures under spilling regular waves, *Coastal Engineering*, 58(2), 151–172.

van der A, D. A., van der Zanden, J., O'Donoghue, T., Hurther, D., Cáceres, I., McLelland, S. J., Ribberink, J. S., 2017. Large-scale laboratory study of breaking wave hydrodynamics over a fixed bar. *Journal of Geophysical Research: Oceans*, 122, 3287-3310, doi:10.1002/2016jc012072.

van der Zanden, J., van der A, D. A., Hurther, D., Cáceres, I., O'Donoghue, T., Ribberink J. S., 2016. Near-bed hydrodynamics and turbulence below a full-scale plunging breaking wave over a mobile barred bed profile, *Journal of Geophysical Research Oceans*, 121, 6482–6506, doi:10.1002/ 2016JC011909.

van der Zanden, J., van der A, D. A., Cáceres, I., Hurther, D., McLelland, S. J., Ribberink, J. S., O'Donoghue, T., 2018. Near-Bed Turbulent Kinetic Energy Budget Under a Large-Scale Plunging Breaking Wave Over a Fixed Bar. *Journal of Geophysical Research: Oceans*, doi:10.1002/2017jc013411

Yoon, H. D., Cox, D. T., 2010. Large-scale laboratory observations of wave breaking turbulence over an evolving beach, *Journal of Geophysical Research*, 115, C10007, doi: 10.1029/2009JC005748.